DOI: 10.61782/fa.2025.0137

FORUM ACUSTICUM
EURONOISE 2025

ANECHOIC NOISE CHARACTERIZATION OF SUB-7KG MULTI-ROTOR DRONES: CONFIGURATION EFFECTS AND SPL SCALING MODELS

Runzhen Cao[1] **Zhicheng Zhang**[1] **Zhenjun Peng** [1]
Zhida Ma[1] **Wangqiao Chen**[1] **Peng Zhou** [1] **Xin Zhang**[1*]
[1] Department of Mechanical and Aerospace Engineering,
The Hong Kong University of Science and Technology,
Clearwater Bay, Kowloon, Hong Kong SAR, China

ABSTRACT

The rapid development of multi-rotor drones has accelerated the growth of the low-altitude economy (LAE), yet expanding applications demand rigorous noise evaluation and regulation due to varying acoustic characteristics across different sizes and configurations. This study investigates the acoustic emissions of sub-7 kg multi-rotor drones during hovering, using both curved and planar phased microphone arrays in an anechoic chamber. Five drone models (0.25 kg to 6.5 kg) were tested to analyze directional noise radiation and spectral behavior. Results show a shift from tonal to broadband-dominant noise as drone size increases, along with lower blade-passing frequencies and smoother directivity patterns in larger platforms. Notably, the heaviest model exhibited lower overall noise than a lighter one, highlighting the impact of aerodynamic design. A logarithmic-linear model incorporating disk area ratio (DAR) was proposed to predict A-weighted sound pressure levels, with strong accuracy ($R^2 > 0.95$) for broadband and overall sound pressure level (SPL). These findings contribute to drone acoustic databases and offer a practical framework for noise prediction, aiding standardization, low-noise design, and regulatory development in urban air mobility. Future work will expand to dynamic flight conditions and other configurations to further enhance model robustness.

*__Corresponding author__: *aexzhang@ust.hk.*

Keywords: *drone noise, multi-rotor acoustics, anechoic measurement, low-altitude economy*

1. INTRODUCTION

With the rapid development of the low-altitude economy (LAE), small multi-rotor drones are increasingly used in logistics, surveillance, and urban mobility [1] . As their deployment expands in urban environments, aerodynamic noise emerges as a key barrier, affecting both human well-being and public acceptance [2] . Accordingly, both the component level and full-vehicle level should be considered, as noise characteristics differ significantly between them. In addition, a standardized noise database and evaluation framework are essential to support drone development, manufacturing, and operational management.

Numerous studies have investigated the aerodynamic noise of drones, particularly from rotor systems. Some have focused on modeling and experimental validation of tonal and broadband noise generated by individual or paired rotors [3, 4] . Others have examined multi-rotor configurations—including coaxial [5, 6] and side-by-side layouts [7–9] —to understand how geometric parameters such as rotor spacing and relative phase affect acoustic performance. In addition, full-vehicle level interactions, including rotor-airframe and rotor-flow coupling effects, have been shown to play a significant role in shaping the overall acoustic behavior of small drones [10–12].

To better reflect realistic flight conditions and capture system-level acoustic effects, recent studies have conducted full-vehicle noise measurements of drones using microphone arrays in both anechoic and outdoor environments. These works typically evaluate key metrics such as

overall sound pressure level (OASPL), blade-passing frequency (BPF) harmonics, broadband noise components, and radiation directivity. Controlled indoor experiments have examined how factors such as observer position, payload, and rotor geometry affect acoustic signatures, while also addressing far-field criteria to ensure the validity of measurements [13, 14] . In contrast, outdoor studies focus on capturing noise during realistic flyover conditions and often employ 3D acoustic field reconstruction techniques [15] . Some investigations further incorporate Geographic Information Systems (GIS)to assess the large-scale environmental impact of drone operations [16] . Together, these efforts underscore the importance of spatially resolved, system-level acoustic measurements and highlight the need for standardized evaluation frameworks to support drone noise regulation and sustainable low-altitude integration.

Although existing studies have improved the understanding of drone noise and informed regulatory efforts, most measurements remain limited to one or two models with narrow variations in size or configuration. To better reflect real-world operations, testing should include larger and more capable drones, as maximum takeoff mass (MTOM) is closely linked to rotor size, configuration layout, and rotational speed—all of which directly influence acoustic performance. For instance, many FAA-approved platforms for advanced operations exceed $5\,\mathrm{kg}$, highlighting the need to study noise behavior in this practically relevant range [17] . While classification systems by EASA, FAA, and CAAC use MTOM thresholds, the category intervals are often too broad to capture meaningful acoustic trends. For example, EU Class C1 includes drones up to $0.9\,\mathrm{kg}$, while C2 extends to $4\,\mathrm{kg}$ [18, 19] . The relationship between drone mass and noise output within these ranges remains poorly understood, motivating higher-resolution measurements across MTOM levels. For untested platforms, anechoic chamber measurements provide a controlled baseline for early-stage acoustic assessment, minimizing environmental interference and supporting consistent noise modeling, design decisions, and policy development [20].

This paper presents a series of acoustic measurements conducted in the anechoic chamber of the Aerodynamics and Acoustics Facility (AAF) at the Hong Kong University of Science and Technology, focusing on typical multi-rotor drones with varying maximum takeoff mass (MTOM) and configurations. The tests were performed under hovering conditions using a curved microphone array to capture noise radiation. Drones under the $7\,\mathrm{kg}$ threshold were selected to span finer MTOM intervals, representing the majority of platforms used in industrial and logistics applications. This work aims to support the sustainable development of the low-altitude economy (LAE), which encompasses drone-based services in logistics, inspection, and urban mobility. To enable cross-platform comparison, dimensionless acoustic parameters were employed to describe noise characteristics within a unified framework. In addition, a logarithmic-linear scaling model incorporating MTOM and disk area ratio (DAR) was developed to predict A-weighted sound pressure levels with high accuracy. The resulting database enhances the understanding of drone acoustics and provides a foundation for future research, regulatory development, and environmentally responsible design.

2. METHODOLOGY

This section outlines the experimental setup for measuring the acoustic emissions of multi-rotor drones under controlled conditions. Five platforms, including both commercial and custom-built models, were selected to represent a range of takeoff weights and configurations relevant to low-altitude operations. Experiments were conducted by using a curved microphone array to capture noise during steady hovering. Measurement feasibility and reliability considerations are also discussed.

2.1 Drone platforms and configurations

Five multi-rotor drones with takeoff masses ranging from approximately $0.25\,\mathrm{kg}$ to $6.5\,\mathrm{kg}$ were selected to represent typical configurations under the $7\,\mathrm{kg}$ threshold. The set includes both commercial and custom-built quadcopters commonly used in consumer, industrial, and commercial applications. All feature a standard X-type layout with two-blade propellers, ensuring structural consistency while varying in frame size, rotor geometry, and propulsion systems. Key physical parameters—such as takeoff mass, propeller diameter, motor spacing, and vertical clearance—are summarized in Tab. 1 . Since most tested platforms are commercial products, only the two custom-built models, X 450 and ZD 680, are shown in Fig. 1.

The selection aligns with regulatory classification systems from EASA, FAA, and CAAC, which define drone categories based on weight. For example, EU categories range from $250\,\mathrm{g}$ (C0) to $4\,\mathrm{kg}$ (C2) [18, 19], FAA defines small UAS under $25\,\mathrm{kg}$ [21], and CAAC classifies drones under $7\,\mathrm{kg}$ as light [22] . This selection increases sam-

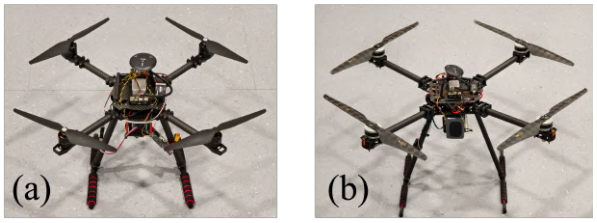

Figure 1. Photographs of the two custom-built platforms: (a) X 450 and (b) ZD 680.

pling density across MTOM levels and configurations, enabling more detailed analysis of acoustic characteristics.

Table 1. Physical parameters of the five tested multirotor drones. "Diag." denotes the diagonal motor-to-motor spacing, "Prop." indicates the propeller diameter, and "Area" refers to the area bounded by the motor layout.

Model	Mass [g]	Diag. [mm]	Prop. [mm]	Clear. [mm]	Area [mm²]
Mini 3	249	247	152	24	39950
Mavic 3	895	380	239	50	74400
X 450	1395	450	254	272	101250
ZD 680	3784	680	432	380	231200
Matrice 350	6470	895	538	239	542700

To better characterize the aerodynamic and geometric properties of the tested drones, the disk area ratio (DAR) was calculated as a dimensionless parameter reflecting the spatial efficiency of the propulsion system. It is defined as the ratio of total rotor swept area to the area enclosed by the motors:

$$\mathrm{DAR} = \frac{n \cdot \frac{\pi D_{\mathrm{prop}}^2}{4}}{A_{\mathrm{enclosed}}} \tag{1}$$

where n is the number of rotors (four in this study), D_{prop} is the propeller diameter, and A_{enclosed} is the area bounded by the motor layout just shown in Tab. 1. Related parameters, including disk loading and layout ratio—which are based on the same core variables such as takeoff mass, propeller diameter, and frame geometry—are also listed in Tab. 2 but are not further analyzed in this study. DAR was later used to develop a scaling model for A-weighted sound pressure levels.

Table 2. Derived parameters of the five tested multirotor drones.

Model	Disk area ratio (DAR)	Disk load	Layout ratio
Mini 3	1.82	10.78	0.62
Mavic 3	2.41	15.67	0.63
X 450	2.00	21.62	0.56
ZD 680	2.54	20.28	0.64
Matrice 350	1.68	22.35	0.60

2.2 Test environment and acoustic measurement setup

All experiments were conducted in the anechoic chamber room. The chamber, measuring $8.1\,\mathrm{m} \times 6.0\,\mathrm{m} \times 5.1\,\mathrm{m}$, is fully wedge-lined and provides free-field conditions above $100\,\mathrm{Hz}$. A nylon safety cage was installed to define an internal working volume of $6.8\,\mathrm{m} \times 4.8\,\mathrm{m} \times 4.0\,\mathrm{m}$, ensuring a minimum $600\,\mathrm{mm}$ clearance from all walls. A net was also placed at the bottom for failsafe protection. High-contrast ground markers were used to support visual-based positioning, especially for lightweight drones operating in GPS-denied indoor environments.

To capture radiated noise under steady hovering, a semi-circular microphone array was deployed at a $2.5\,\mathrm{m}$ radius from the chamber center. The array spanned a $120°$ vertical arc and consisted of thirteen GRAS 46BE 1/4-inch microphones, spaced at $10°$ intervals. The vertical angle of each microphone is denoted by θ, measured from the downward vertical direction ($\theta = 0°$) upward toward the drone's front axis. This angular configuration allows for directional analysis of noise radiation.The array was tilted $60°$ from the chamber's short axis, with the central microphone aligned to the drone's nominal hovering position. Each microphone was fitted with a windscreen to reduce flow-induced noise. A schematic and chamber photo are shown in Fig. 3 and Fig. 2 , including microphone locations, coordinate systems, and marker placement. Drone position and yaw were tracked by a VICON

system with eight Vero V2.2 cameras operating at 50 Hz , using reflective markers beneath each rotor and on the airframe. The system was synchronized with acoustic measurements acquired via NI cDAQ-9189 and NI-9231 modules at 50 kHz . To minimize acoustic interference, metal components of the safety cage were acoustically treated with foam.

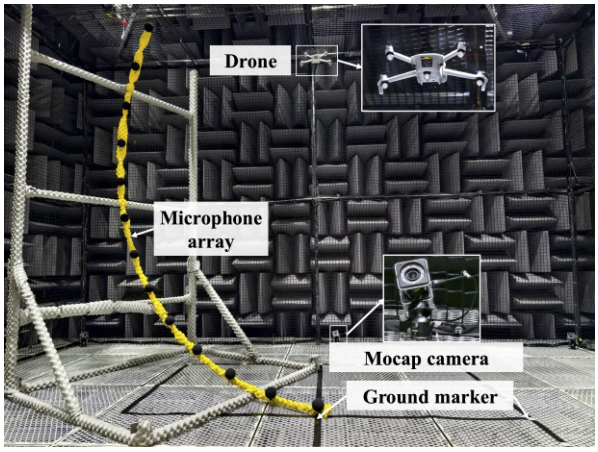

Figure 2. Experimental setup in the AAF anechoic chamber room.

2.3 Test procedure and evaluation of measurement validity and repeatability

Each drone was tested under consistent procedures to characterize its directional acoustic behavior. The drone hovered at the geometric center of the chamber, 2.5 m above the floor (Fig. 3), and was rotated about its vertical body axis (z_b) from 0° to 180° in 15° increments. At each orientation, a 20 s recording was made using synchronized systems: acoustic signals were captured at 50 kHz by the 13-microphone array, while position and yaw were tracked at 50 Hz via the VICON system. Each drone completed three full test cycles to evaluate repeatability.

Measurement validity was ensured through chamber background noise checks and array configuration validation. Ambient noise levels were maintained below 20 dB across the frequency range of interest to achieve sufficient signal-to-noise ratio. The microphone array design was evaluated against ISO 3745:2012 [23] far -field criteria. For the largest drone, Matrice 350 RTK ($L = 1.433$ m), the array radius fell slightly short of the $2L$ condition but exceeded other requirements [14], with a 13 % deviation

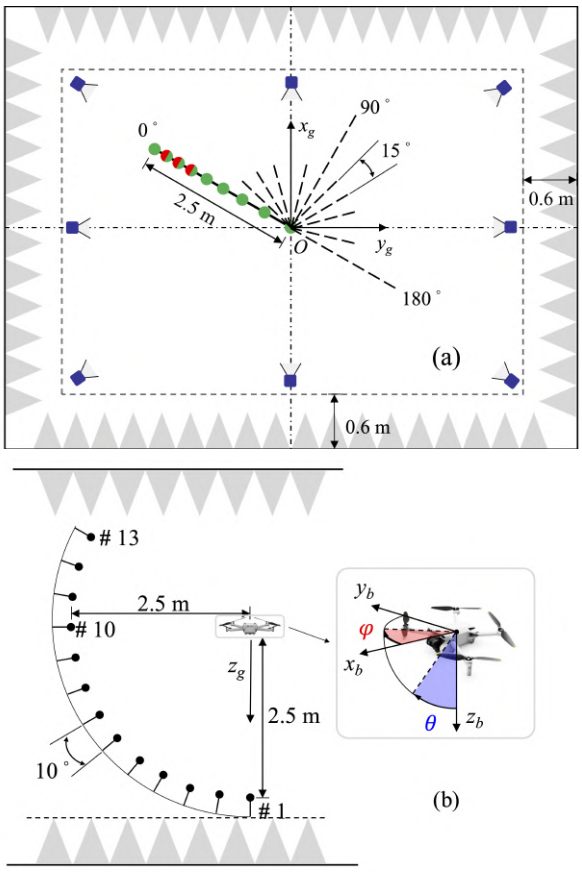

Figure 3. Schematic diagrams of the acoustic measurement setup: (a) top view showing the microphone array orientation; (b) side view including the drone body coordinate system.

deemed acceptable. All smaller drones fully met the criteria. Additionally, the influence of rotor downwash and recirculating flow was considered. Previous studies [24] indicate that such effects cause minor spectral shifts and entropy changes, but their impact on A-weighted broadband SPL remains within 2 dB , and thus does not compromise measurement reliability.

3. RESULTS AND DISCUSSIONS

This section presents the acoustic analysis of all tested multi-rotor drones during steady hovering. Each platform was incrementally rotated in yaw, and sound pressure levels were recorded at 13 microphone positions along a 120°

vertical arc. The signals were post-processed to extract A-weighted overall sound pressure levels (OASPL), narrowband SPL spectra, and directional features, including 2D directivity plots and interpolated 3D fields. The analysis focuses on identifying shared acoustic characteristics across platforms, yaw-dependent frequency behaviors, and trial-to-trial consistency. In addition, scaling relationships between A-weighted OASPL and maximum takeoff mass (MTOM) are evaluated to investigate how noise radiation evolves with platform size.

3.1 Hovering stability evaluation via motion capture

To assess the hovering stability of the tested multi-rotor drones, we analyzed the standard deviation of body center positions and yaw angles during a steady 20-second hover at $0°$ yaw, as summarized in Tab. 3. All five platforms maintained sub- $6\,\mathrm{mm}$ deviations across all spatial axes. The Matrice 350 exhibited the most stable performance, with variations under $3\,\mathrm{mm}$ and minimal yaw fluctuation ($0.77°$). In contrast, the ZD 680 showed the largest vertical ($3.42\,\mathrm{mm}$) and yaw ($1.16°$) deviations, which may be attributed to increased inertia or less refined control tuning. The Mini 3 displayed slightly larger vertical fluctuation ($5.16\,\mathrm{mm}$), likely due to its lower mass and greater susceptibility to recirculating flow , although further testing would be required to confirm this. Overall, all platforms demonstrated sufficient stability to support repeatable and reliable indoor acoustic measurements.

Table 3. Standard deviation of motion capture measurements under hovering at $0°$ yaw for each drone model (unit: mm / °).

Model	X std [mm]	Y std [mm]	Z std [mm]	Yaw std [°]
Mini 3	3.47	2.56	5.16	0.92
Mavic 3	3.13	2.61	2.69	1.06
X 450	3.65	2.96	3.71	0.93
ZD 680	5.06	3.31	3.42	1.16
Matrice 350	2.66	1.99	2.12	0.77

3.2 Acoustic characteristics analysis

Acoustic analysis was based on signals recorded at a microphone positioned at $\theta = 30°$, oriented perpendicular to the drone's forward axis. This angle was selected because the bottom-mounted microphone, affected by rotor downwash, failed to clearly capture tonal components such as the first blade-passing frequency (BPF) . The $30°$ position provided a more representative signal across platforms. Given the presence of multiple tonal peaks around BPFs due to rotor asymmetry and aerodynamic interactions, each BPF in this study is defined as a frequency band rather than a single frequency. The reported SPL values represent the A-weighted energy integrated over each corresponding band.

The A-weighted narrowband SPL spectra of the five drones under hover are shown in Fig. 4 . The Mini 3 exhibits the lowest SPL, with acoustic energy concentrated in the low-frequency region, while the Mavic 3 and X 450 display stronger tonal peaks in the mid-frequency range. The heavier ZD 680 and Matrice 350 generate higher SPL across a broader spectral range (1–6 kHz), consistent with their greater thrust demand and more complex aerodynamic interactions. As maximum takeoff mass (MTOM) increases, the spectra become increasingly broadband, with relatively diminished tonal peaks, broader spectral ridges, and lower blade-passing frequencies. These trends suggest more distributed and diffuse acoustic signatures in larger drones. Design asymmetries such as staggered rotor heights or center-of-mass offsets may further suppress tonal coherence and reduce directional radiation. All spectra remain well above the background noise floor, confirming measurement fidelity.

Fig. 5 illustrates the relationship between maximum takeoff mass (MTOM) and A-weighted SPL across multiple frequency bands, including 1BPF, 2BPF, 3BPF, broadband, and overall. In general, SPL increases with MTOM across all bands, with the most pronounced growth observed at 1BPF and 2BPF, reflecting stronger tonal components in heavier platforms. Broadband and higher-order components exhibit a more gradual increase, suggesting a more distributed energy spectrum. An exception to this trend is the Matrice 350, which, despite its higher MTOM compared to the ZD 680, exhibits slightly lower A-weighted SPL across all metrics—likely due to noise reduction measures such as optimized propeller geometry and a more aerodynamically refined fuselage.

The observed trends in A-weighted SPL are further visualized in Fig. 6 , which presents 3D directivity maps

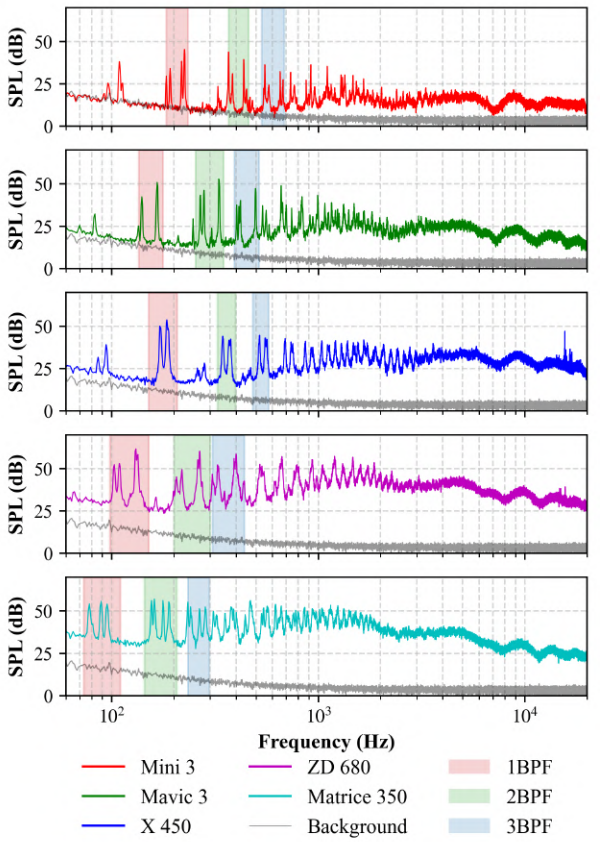

Figure 4. Comparison of SPL spectra measured at the $\theta = 30°$ microphone for all drones under hover condition. The shaded regions represent the respective BPF bands.

of A-weighted OASPL for all five platforms. The X 450 exhibits a fragmented and irregular radiation pattern, likely resulting from structural resonance and less coherent rotor interaction. In contrast, the ZD 680 shows a well-defined downward lobe with elevated levels, reflecting high rotor loading and more focused downward radiation. The Matrice 350, despite its larger size, displays a smooth and symmetric pattern with noticeably lower peak levels, consistent with its overall reduced SPL observed in Fig. 5 . These results suggest that aerodynamic refinements—such as smoother fuselage contours and optimized propeller design—can effectively mitigate directional noise radiation even in larger multirotor systems.

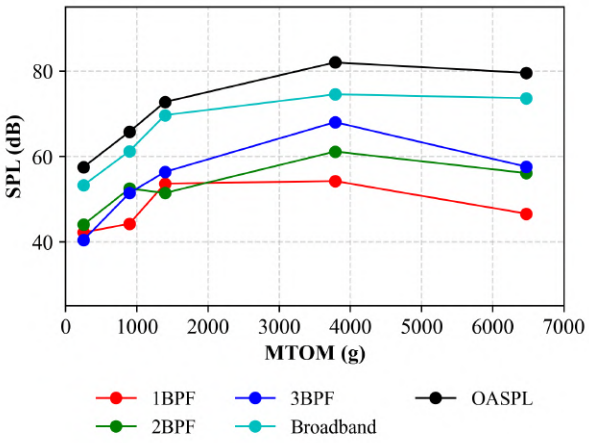

Figure 5. Variation of A-weighted Sound Pressure Level (SPL) with Maximum Takeoff Mass (MTOM) across different frequency bands: 1BPF, 2BPF, 3BPF, Broadband, and OASPL.

3.3 Model fitting and data analysis

To characterize how A-weighted SPL varies with platform mass and configuration, we adopted a logarithmic-linear model incorporating disk area ratio (DAR). This model provides a more accurate representation of the noise emissions across different frequencies using the following equation(2):

$$\mathrm{SPL} = a \cdot \ln(\mathrm{MTOM}) + b \cdot \mathrm{MTOM} + c \cdot \mathrm{DAR} + d \quad (2)$$

Due to the higher variability and less consistent results at blade-passing frequencies (1BPF–3BPF), and given that OASPL is easier to manage and unify in regulatory contexts, we focused our analysis on Broadband SPL and OASPL. The fitted parameters for all frequency bands are summarized in Tab. 4.

4. CONCLUSION

This study examined the acoustic characteristics of multirotor drones with varying maximum takeoff masses and configurations under controlled hovering conditions. Results show that A-weighted sound pressure levels (SPL) scale with drone mass. To quantify the influence of mass and geometry, a logarithmic-linear model incorporating disk area ratio (DAR) was developed to predict A-weighted SPL across frequency bands, achieving strong

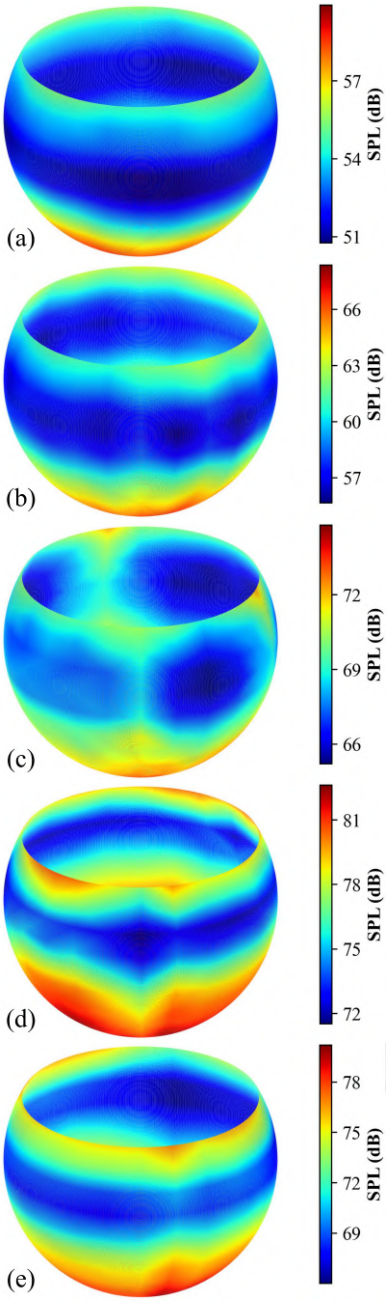

Figure 6. A-weighted OASPL directivity maps from a 45° view: (a) Mini 3, (b) Mavic 3, (c) X 450, (d) ZD 680, (e) Matrice 350.

accuracy for broadband and overall levels. These findings contribute a standardized acoustic dataset and modeling approach that support low-noise drone design, regulatory development, and integration into urban air mobility. Future work will extend to dynamic flight conditions, transitional states, and a broader range of configurations to improve the generalizability of the predictive model and facilitate sustainable development of the low-altitude economy.

Table 4. Fitted coefficients for the A-weighted SPL log-linear model defined in (2), incorporating maximum takeoff mass (MTOM) and disk area ratio (DAR). "B'band." refers to broadband SPL.

P.	1BPF	2BPF	3BPF	B'band.	OASPL
a	9.521	2.897	9.555	11.66	9.273
b	-3.83 $\times 10^{-3}$	7.10 $\times 10^{-4}$	-1.63 $\times 10^{-3}$	-2.60 $\times 10^{-3}$	-9.10 $\times 10^{-4}$
c	-2.589	8.991	8.461	-2.890	2.060
d	-6.260	11.227	-28.65	-6.118	1.737
R^2	0.6858	0.9942	0.9348	0.9628	0.9574

5. ACKNOWLEDGMENTS

This work was supported by the Hong Kong Research Grant Council (RGC 16201923 and 16202519).

6. REFERENCES

[1] X. Huang, "The small-drone revolution is coming — scientists need to ensure it will be safe," *Nature*, vol. 637, pp. 29–30, Jan. 2025.

[2] B. Schäffer, R. Pieren, K. Heutschi, J. M. Wunderli, and S. Becker, "Drone Noise Emission Characteristics and Noise Effects on Humans—A Systematic Review," *International Journal of Environmental Research and Public Health*, vol. 18, p. 5940, June 2021.

[3] H. Wu, P. Zhou, P. Wang, G. Zhou, B. Chen, S. Zhong, and X. Zhang, "Broadband noise of a hovering rotor: Measurement, prediction, and reduction," *AIAA Journal*, vol. 0, no. 0, pp. 1–13, 0.

[4] X. Li, H. Wu, Y. Li, P. Zhou, S. Zhong, X. Zhang, and Z. Ma, "Experimental study of the effect of boundary-layer transition on rotor aeroacoustics," *AIAA Journal*, vol. 62, no. 5, pp. 1974–1981, 2024.

[5] R. S. McKay, M. J. Kingan, S. T. Go, and R. Jung, "Experimental and analytical investigation of contra-rotating multi-rotor uav propeller noise," *Applied Acoustics*, vol. 177, p. 107850, 2021.

[6] W. Chen, Z. Ma, Étienne Spieser, J. Guo, P. Zhou, S. Zhong, X. Zhang, and X. Huang, "Acoustic imaging of the broadband noise arising in contra-rotating co-axial propellers," *Aerospace Science and Technology*, vol. 141, p. 108531, 2023.

[7] X. Xu, Y. Lu, C. Lan, M. Shao, and J. Lu, "Mechanism analysis of the influence of rotor-to-rotor interactions on global rotor noise," *Journal of Sound and Vibration*, vol. 585, p. 118473, 2024.

[8] H. Bu, H. Wu, C. Bertin, Y. Fang, and S. Zhong, "Aerodynamic and acoustic measurements of dual small-scale propellers," *Journal of Sound and Vibration*, vol. 511, p. 116330, 2021.

[9] K. A. Pascioni, S. A. Rizzi, and N. Schiller, "Noise Reduction Potential of Phase Control for Distributed Propulsion Vehicles," in *AIAA Scitech 2019 Forum*, (San Diego, California), American Institute of Aeronautics and Astronautics, Jan. 2019.

[10] S. Cantos, P. Zhou, Z. MA, and Y. Li, *A Numerical Study on the Reduction of Rotor Blade-Airframe Interaction Noise Through Airframe Permeability*.

[11] J. Whelchel and W. N. Alexander, *sUAS Rotor-Airframe Interaction*.

[12] J. Wu, O. Stalnov, W. Chen, Z. Yang, and X. Huang, "Transient analysis of blade-vortex interaction noise," *Aerospace Science and Technology*, vol. 120, p. 107294, 2022.

[13] M. Alkmim, J. Cardenuto, E. Tengan, T. Dietzen, T. Van Waterschoot, J. Cuenca, L. De Ryck, and W. Desmet, "Drone noise directivity and psychoacoustic evaluation using a hemispherical microphone array," *The Journal of the Acoustical Society of America*, vol. 152, pp. 2735–2745, 11 2022.

[14] Z. Ma, H. Wu, J. Mao, G. Liu, P. Zhou, and S. Zhong, "Noise measurement of a quadrotor drone in an anechoic chamber," *INTER-NOISE and NOISE-CON Congress and Conference Proceedings*, vol. 268, pp. 4659–4670, Nov. 2023.

[15] C. Ramos-Romero, N. Green, A. J. Torija, and C. Asensio, "On-field noise measurements and acoustic characterisation of multi-rotor small unmanned aerial systems," *Aerospace Science and Technology*, vol. 141, p. 108537, 2023.

[16] F. Škultéty, E. Bujna, M. Janovec, and B. Kandera, "Noise impact assessment of uas operation in urbanised areas: Field measurements and a simulation," *Drones*, vol. 7, no. 5, 2023.

[17] F. A. Administration, "Nepa and drones: Guidance for environmental review of uas operations," 2023.

[18] E. Commission, "Commission delegated regulation (eu) 2019/945 of 12 march 2019 on unmanned aircraft systems and on third-country operators of unmanned aircraft systems," 2019.

[19] E. Commission, "Commission delegated regulation (eu) 2020/1058 of 27 april 2020 amending delegated regulation (eu) 2019/945 as regards the introduction of two new unmanned aircraft systems classes," 2020.

[20] T. Zhou, H. Jiang, and B. Huang, "Quad-copter noise measurements under realistic flight conditions," *Aerospace Science and Technology*, vol. 124, p. 107542, 2022.

[21] "14 cfr part 107: Small unmanned aircraft systems." `https://www.ecfr.gov/current/title-14/chapter-I/subchapter-F/part-107`, 2024. Accessed: 2025-04-03.

[22] "Interim regulations on unmanned aircraft flight management." `https://www.caac.gov.cn/XXGK/XXGK/FLFG/202401/t20240115_222642.html`, 2023. In Chinese; Accessed: 2025-04-03.

[23] International Organization for Standardization, "Acoustics – determination of sound power levels and sound energy levels of noise sources using sound pressure – precision methods for anechoic rooms and hemi-anechoic rooms," Standard ISO 3745:2012, International Organization for Standardization, Geneva, CH, 2012.

[24] Z. Ma, P. Zhou, X. Zhang, and S. Zhong, "Experimental assessment of the flow recirculation effect on the noise measurement of a free-flying multi-rotor uas in a closed anechoic chamber," *Acoustics Australia*, pp. 1–10, 2024.